DELAMINATION QUANTIFICATION IN A CROSS-PLY LAMINATE BASED ON TOPOLOGY OPTIMIZATION AND LAMB WAVE PROPAGATION MECHANISMS

Kazuki Ryuzono[1], Shigeki Yashiro[2], Sota Onodera[3], Nobuyuki Toyama[4] and Tomonaga Okabe[5]

[1] Department of Aerospace Engineering, Tohoku University, 6-6-01, Aramaki-Aza-Aoba, Aoba-ku, Sendai, Miyagi 980-8579, Japan, ryuzono@tohoku.ac.jp
[2] Department of Aeronautics and Astronautics, Kyushu University, 744 Motooka, Nishi-ku, Fukuoka, Japan, yashiro@aero.kyushu-u.ac.jp
[3] Department of Aeronautics and Astronautics, Kyushu University, 744 Motooka, Nishi-ku, Fukuoka, Japan, sota.onodera@aero.kyushu-u.ac.jp
[4] National Metrology Institute of Japan, National Institute of Advanced Industrial Science and Technology (AIST), 1-1-1 Umezono, Tsukuba, Ibaraki, Japan, toyama-n@aist.go.jp
[5] Department of Aerospace Engineering, Tohoku University, 6-6-01, Aramaki-Aza-Aoba, Aoba-ku, Sendai, Miyagi 980-8579, Japan, tomonaga.okabe.a8@tohoku.ac.jp

Keywords: Non-destructive evaluation, Damage identification, Delamination, Topology optimization, Ultrasonic visualization

ABSTRACT

This study experimentally visualized Lamb waves propagating in a film-inserted cross-ply laminate and applied a topology-optimization-based damage identification method to the experimental results to discuss its feasibility. In this method, delamination was estimated as a distribution of damage parameters that reproduced the experimentally visualized Lamb wave propagation in an inverse analysis model. The damage parameters were set to the internal residual strength variables controlling the traction of cohesive elements. When maximum amplitudes were evaluated in the objective function of the topology optimization problem, the present method successfully identified the complex shape of the film-inserted region by utilizing standing waves propagating perpendicular to the surface fiber orientation in the delaminated area. Conversely, the present method did not identify the film-inserted area by evaluating only the maximum amplitudes of the Lamb waves propagating parallel to the surface fiber orientation. Therefore, the numerical experiments were performed to discuss the ultrasonic features evaluated in the objective function, and the delaminated region was successfully estimated by evaluating whole time of the Lamb wave signal at each node even when the Lamb waves propagated parallel to the surface fiber orientation. These results demonstrate that the present method can quantitatively evaluate delamination by incorporating the ultrasonic features highly sensitive to delamination into the objective function.

1 INTRODUCTION

Quantitative ultrasonic non-destructive evaluation is essential to ensure the reliability of composite structures during long-term operation. Identifying delamination generated in carbon-fiber-reinforced plastic (CFRP) laminates subjected to out-of-plane impact is particularly important because delamination significantly reduces the residual compressive strength of composite structures. Ultrasonic C-scan inspection has been generally applied to delamination inspection; however, the C-scan system requires inspection targets to be immersed in water and time-consuming mechanical scanning over a wide area. Therefore, previous studies [1,2] developed a laser scanning system to visualize ultrasonic waves and detected delamination more easily and quickly than the C-scan. Nonetheless, visualized ultrasonic waves in thin CFRP laminates included various Lamb wave modes [3] generated by unknown damage and medium boundaries, which resulted in difficulties in interpreting the visualized waves and evaluating delamination sizes and shapes. To overcome the difficulties, numerous studies [4] have incorporated signal processing, feature extraction, and inverse analysis techniques into the ultrasonic imaging system, and this system still needs to be further improved to evaluate delamination quantitatively and reliably.

Topology optimization [5] is promising for an inverse analysis to quantitatively assess complex damage sizes and shapes in composite structures because it can estimate a distribution of materials. Niemann et al. [6] used topology optimization and evaluation of the natural frequencies to estimate out-of-plain impact-induced delamination. However, the global vibration characteristics did not have enough information to identify the sizes and shapes of local delamination with high accuracy. Conversely, the visualized ultrasonic wave propagation contains rich data in two-dimensional space and one-dimensional time domains. The authors [7,8] proposed a damage identification method by introducing topology optimization into the ultrasonic visualization system and successfully identified penetrated small cracks in metal plates in actual inspections. However, the proposed method was still not applied to delamination evaluation in CFRP laminates.

Therefore, this study experimentally visualized Lamb wave propagation in a delaminated CFRP laminate and applied the topology-optimization-based damage identification method to the experimental results, and its feasibility was discussed. In the present method, delamination was simulated by cohesive elements, and damage parameters, i.e., design variables in the topology optimization problem, were set to the internal residual strength variables controlling the traction of the cohesive elements. A film-inserted area in a cross-ply laminate was estimated as the distribution of the damage parameters, and appropriate ultrasonic features to be evaluated in the objective function were discussed to identify delamination with an unknown location.

2 EXPERIMENTS

2.1 Materials and measurements

A cross-ply laminate with a stacking sequence of $[0_4/90_4]_S$ was prepared to be inspected. The material used was a CFRP (T700SC/2592, Toray), and the laminate dimensions were 160 mm × 160 mm × 2 mm. Two layers of polyimide films (Kapton®, DuPont) with dimensions of 10 mm × 10 mm × 0.03 mm were inserted in the center of one 0/90° interface to introduce artificial delamination. The C-scan image (Figure 1a) exhibited the film-inserted area. This artificial delamination was the identification target of the present method.

Figure 1b shows a photograph of the laser Doppler vibrometer (LDV) scanning system to visualize Lamb wave propagation. In this system, five-period 200-kHz sinusoidal waves multiplied by a Hanning window were created by a multi-functional generator (WF1974, NF Corporation). The waves were amplified through a high-speed bipolar amplifier (BA4825, NF Corporation) and were excited by a piezoelectric transducer (PW B0.2K20N, Japan Probe) in contact with the laminate. At a 200-kHz resonance frequency of the transducer, the waves propagated as only fundamental Lamb modes (S0 and A0 modes) in the laminate used in this study. The inspection area on the laminate was scanned by LDV (PSV-500-M, Polytec), and the out-of-plane velocity at each illuminated point was measured on the Doppler effect. The measured waves were bandpass-filtered from 50 to 400 kHz and were collected on a computer using a data acquisition board (PCI-6110, National Instruments). The out-of-plane displacement was calculated by integrating the out-of-plane velocity. The video of Lamb waves propagating through the laminate was obtained by plotting the amplitude of the out-of-plane displacement on a contour map in the order of the measurement time.

Figure 1c shows a schematic diagram of measurement conditions. A 50 mm × 50 mm region on the surface nearer the film-inserted interface was scanned with a scan spacing of 0.5 mm (101 × 101 points). Two visualized Lamb wave propagation in the parallel (incident angle $\theta = 0°$) and perpendicular ($\theta = 90°$) directions to the surface fiber orientation were measured to discuss the identification results at different incident angles to the delamination. The transducer was fixed 40 mm away from the center of the film-inserted area. The measurement time was 100 μs. To improve the signal-to-noise ratio of the LDV, the inspection area was painted white, and the ultrasonic signals measured ten times at each scanned point were averaged.

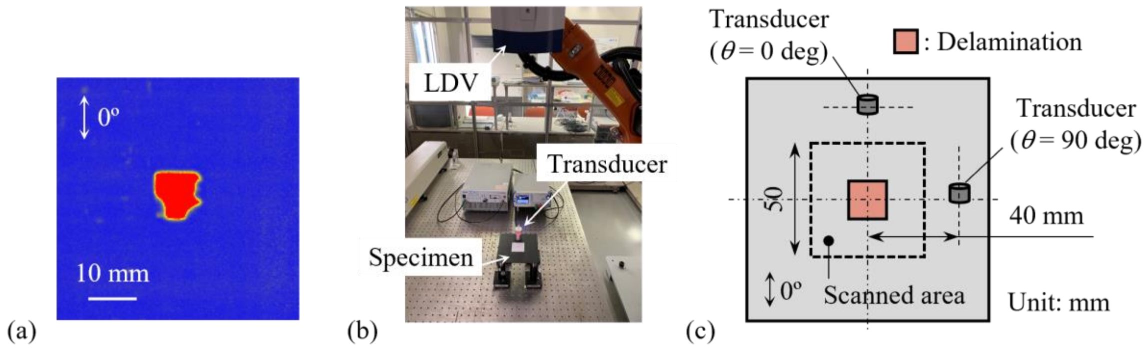

Figure 1: Materials and measurements of the experiment: (a) the C-scan image of film-inserted cross-ply laminate, (b) photograph of laser Doppler vibrometer scanning system, and (c) laser scanning area and fixed transducer position at 0° and 90° incident angles.

2.2 Measurement results

Figure 2 shows the snapshots of the visualized Lamb wave propagation in the film-inserted laminate. Although the incident S0 and A0 mode waves were observed, this study focused on the A0 mode because the out-of-plane displacement of the S0 mode was small. The phase delay of the A0 mode was observed in the film-inserted area (the snapshots at 57 μs). This is because the entire laminate $[0_4/90_4]_S$ was divided into two sub-laminates $[0_4]_T$ and $[90_8/0_4]_T$ by the delamination, and the A0 mode velocity in the delaminated area (e.g., $[0_4]_T$) differed from the one in the intact area (e.g., $[0_4/90_4]_S$) owing to the dispersive nature of Lamb waves. Moreover, the A0 mode waves were repeatedly reflected at the delamination edges and remained as standing waves in the delaminated region even after passing through the delaminated area (the snapshots at 67 μs). The reflections were required for the A0 modes in the sub-laminates to pass through the delamination edge aligning their phases [9]. These phenomena were observed regardless of the incidence angles.

Maximum-amplitude maps exhibited characteristic distributions owing to delamination [2,10,11]. Therefore, the maps, as shown in Figure 3, were obtained by extracting the maximum-amplitude values from the visualized wave propagation results at each scanned point in a 20 mm × 20 mm area (inside the dashed square in the snapshots at 67 μs). The maximum-amplitude values were high in the film-inserted area regardless of the incident angles. The film-inserted area was characterized by the high-amplitude area in the case of θ = 90°, whereas the intact area exhibited as high amplitude as the delaminated one in the case of θ = 0°, resulting in not identifying the delamination sizes and shapes.

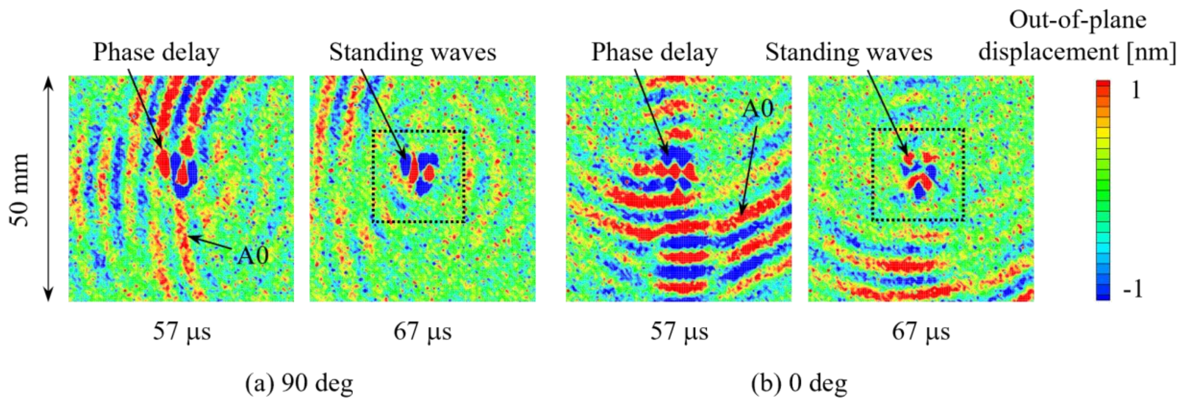

Figure 2: Experimentally visualized Lamb wave propagation (out-of-plane displacement) on the film-inserted cross-ply laminate.

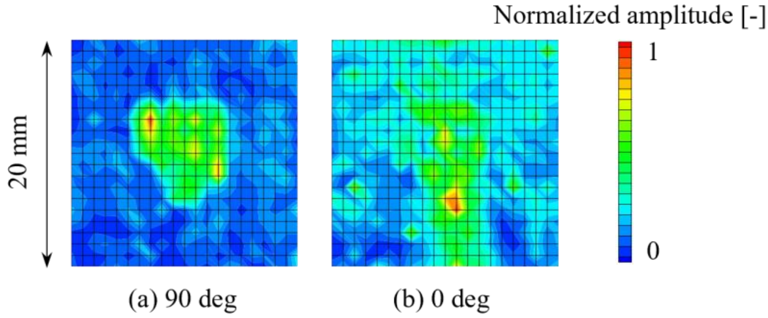

Figure 3: Maximum amplitude maps of the experimentally visualized Lamb wave propagation (out-of-plane displacement) on the film-inserted cross-ply laminate.

3 DELAMINATION IDENTIFICATION APPROACH

3.1 Formulation

The topology-optimization-based damage identification method combined with the ultrasonic visualization estimates damage as a distribution of damage parameters that reproduces visualized ultrasonic wave propagation in an inverse analysis model. In this section, the topology optimization problem including the damage parameters and objective function is set to estimate delamination.

In the inverse model used in this study, delamination is simulated by one-parameter cohesive elements [12]. The traction T_i of the cohesive element i is expressed as follows:

$$T_i^m(s_i) = \frac{s_i}{1-s_i}\frac{\tau^{m,\max}}{\Delta^{mc}}\Delta_i^m \quad \text{for } m = n,t,b \tag{1}$$

where Δ is the relative displacement, and the superscripts n, t and b indicate the deformation modes I, II and III. $\tau^{m,\max}$ and Δ^{mc} are the strength and critical relative displacement. s_i is the internal residual strength variable. The initial value s_{ini} (0.9) and 0 represent intact and perfectly delaminated. Therefore, in the present method, the internal residual strength variable s_i of the cohesive element i in the design domain D is adopted as the damage parameter as follows:

$$s_i = \begin{cases} 0 & \text{for } i \in \Omega_d \\ s_{\mathrm{ini}} & \text{for } i \in D \setminus \Omega_d \end{cases} \tag{2}$$

where Ω_{d} and $D \setminus \Omega_{\mathrm{d}}$ are the delaminated and intact regions, respectively. The damage parameter s_i takes a continuous value from 0 to s_{ini} and indicates the severity of delamination.

Dynamic finite element analysis of wave propagation is performed in the inverse analysis model, and the optimization problem is defined as the minimization of the sum of the squared error between the estimated ultrasonic feature $\boldsymbol{U}_{\mathrm{FEM}}(\boldsymbol{s})$ and the target one $\boldsymbol{U}_{\mathrm{target}}$, as follows:

$$\min_{\boldsymbol{s}} f(\boldsymbol{s}) = \sum_{j=1}^{M}\left(U_{\mathrm{FEM},j}(\boldsymbol{s}) - U_{\mathrm{target},j}\right)^2 \tag{3}$$

$$\text{subject to} \quad 0 \le s_i \le s_{\mathrm{ini}} \quad \text{for } i = 1,\cdots N \tag{4}$$

where M and N are the number of the nodes j and cohesive elements i in the design domain D, respectively.

In the abovementioned procedure, the optimal damage parameter $\boldsymbol{s}^*$ is estimated. The damage parameter $\boldsymbol{s}$ is updated by sequential quadratic programming, and the gradient of the objective function is calculated by the forward finite difference method. To reduce computational costs, the upper limit of the optimization step k is set to 30. The initial value of the damage parameter $\boldsymbol{s}^0$ is set to s_{ini}.

3.2 Inverse analysis model

Figure 4 shows the inverse analysis model. The model of dimensions 80 mm × 80 mm × 2 mm was discretized using eight-node hexahedral solid elements of dimensions 1 × 1 × 0.25 mm. The stacking sequence was $[0_4/90_4]_S$, and a 0/90° interface adhered by cohesive elements [12] to simulate delamination. The model included 51200 solid elements, 6400 cohesive elements and 65610 nodes. The properties [13,14] of the CFRP and cohesive elements used in this model are listed in Table 1. A five-period 200-kHz sinusoidal-wave load multiplied by a Hanning window was applied in the through-thickness direction to a 10 mm radius region of the fixed transducer position in the experiments. All remaining boundaries were free edges. The time step for the dynamic finite element analysis was 0.01 µs, which satisfied the Courant condition. The design domain D for the topology optimization was a 20 mm × 20 mm area in the center of the inverse analysis model. All damage parameters of the cohesive elements in the other regions were fixed at s_{ini}.

The Lamb wave propagation analysis was performed with s_i = 0 and s_{ini} in the central 10 mm × 10 mm (10 × 10 elements) and remaining regions in the design domain, respectively. Figure 5 shows the numerical results of the visualized wave propagation obtained by plotting the out-of-plane displacement at the nodes on the inspected surface as shown in Figure 4. Regardless of the incidence angles, the phase delay and standing waves of the A0 mode were observed in the delaminated region. The high-amplitude region in the maximum-amplitude map at θ = 90° (Figure 6a) characterized the delaminated area, whereas the delaminated region was not identified at θ = 0° (Figure 6b). These numerical results were consistent with the measurement results (Figures 2 and 3). Therefore, the maximum-amplitude maps were adopted as the ultrasonic feature $\boldsymbol{U}_{\mathrm{FEM}}(\boldsymbol{s})$ and $\boldsymbol{U}_{\mathrm{target}}$ in the objective function in this study.

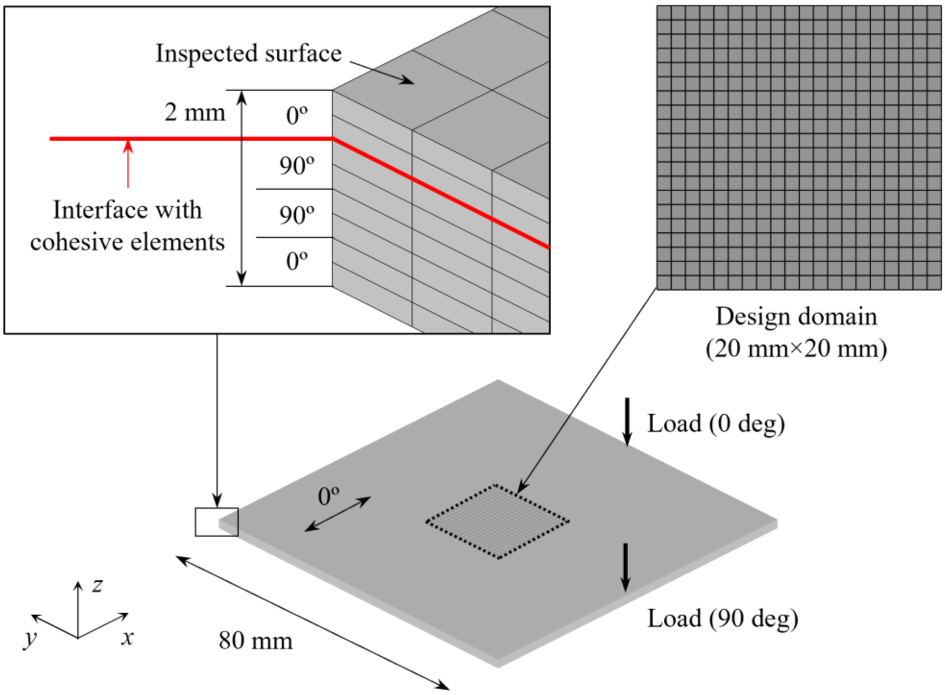

Figure 4: Inverse analysis model with cohesive elements for a cross-ply laminate.

Table 1: Properties of CFRP (T700SC/2592) laminate and cohesive elements [13,14].

Material properties of CFRP (T700SC/2592) laminate	
Longitudinal Young's modulus [GPa]	132
Transverse Young's modulus [GPa]	9.85
In-plane shear modulus [GPa]	5.25
Out-of-plane shear modulus [GPa]	3.80
In-plane Poisson's ratio [-]	0.25
Out-of-plane Poisson's ratio [-]	0.38
Density [g/cm^3]	1.80
Properties for cohesive elements	
In-plane tensile strength (Mode I) [MPa]	85.9
In-plane shear strength (Mode II) [MPa]	60.0
Out-of-plane shear strength (Mode III) [MPa]	60.0
Critical energy release rate (Mode I) [kJ/m2]	0.244
Critical energy release rate (Mode II) [kJ/m2]	1.06
Critical energy release rate (Mode III) [kJ/m2]	1.06

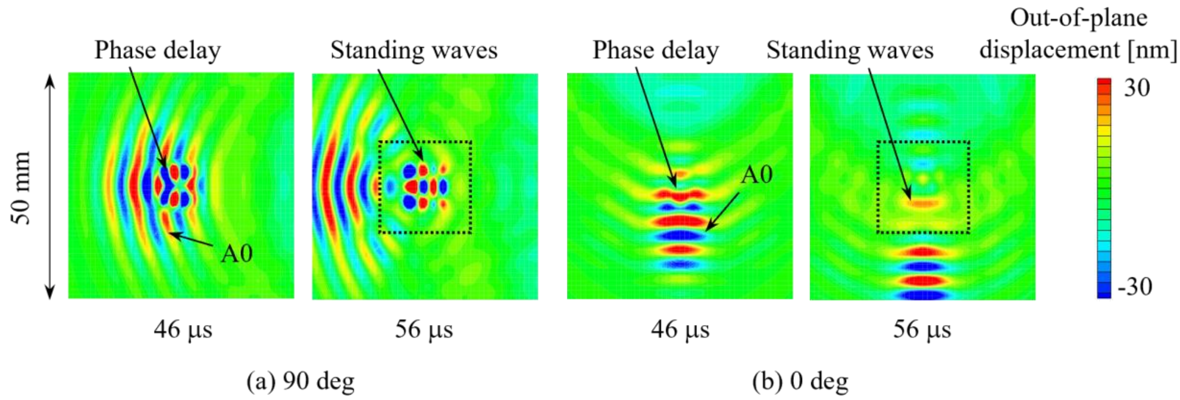

Figure 5: Numerical results of Lamb wave propagation (out-of-plane displacement) on the inverse analysis model.

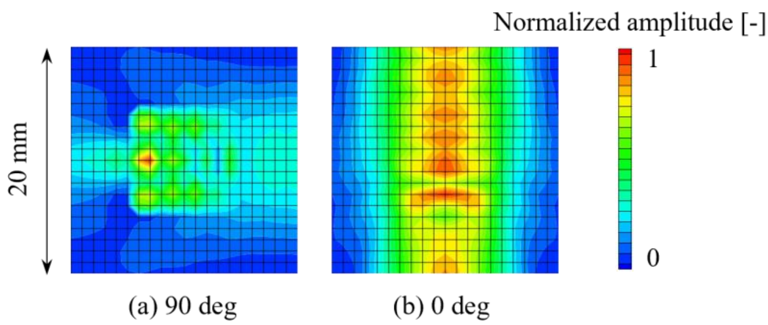

Figure 6: Maximum amplitude map of Lamb wave propagation (out-of-plane displacement) on the inverse analysis model.

4 RESULTS AND DISCUSSION

4.1 Delamination identification results

Figure 7 shows the optimal damage parameter distribution $\boldsymbol{s}^*$ and maximum-amplitude map $\boldsymbol{U}_{\mathrm{FEM}}(\boldsymbol{s}^*)$ compared to the target. In the case of $\theta = 90°$, the damage parameters in the film-inserted region were much smaller than that in the intact region, and the estimated maximum-amplitude map $\boldsymbol{U}_{\mathrm{FEM}}(\boldsymbol{s}^*)$ well reproduced the $\boldsymbol{U}_{\mathrm{target}}$. These results demonstrate that the present method is applicable to identifying the complex delamination shape by utilizing the standing waves propagating at $\theta = 90°$. Conversely, in the case of $\theta = 0°$, the damage parameters in the intact area of the target were also small, and the film-inserted area was not identified. The $\boldsymbol{U}_{\mathrm{FEM}}(\boldsymbol{s}^*)$ did not agree as well with the $\boldsymbol{U}_{\mathrm{target}}$, as compared to $\theta = 90°$. Figure 8 shows the change in the objective function during the optimization process. The objective function was not closer to zero for $\theta = 0°$ compared to $\theta = 90°$. This result shows that the estimated damage parameter distribution in the case of $\theta = 0°$ was one of the local optimal solutions. Comparing the maximum-amplitude maps for the initial and optimized damage parameters, $\boldsymbol{s}^0$ and $\boldsymbol{s}^*$, there was no significant change for $\theta = 0°$, although the high-amplitude area changed significantly for $\theta = 90°$. Therefore, the maximum-amplitude map for $\theta = 0°$ did not change significantly even if the delamination distribution changed, i.e., the sensitivity of the objective function was low for $\theta = 0°$.

In the previous study [11], when an entire laminate was divided into two sub-laminates by delamination, standing waves with high amplitudes were generated in the sub-laminate with a smaller flexural stiffness in the wave propagation direction than the other sub-laminate. This phenomenon was observed particularly when the sub-laminates above and below the delamination had considerably different flexural stiffnesses. Therefore, the standing waves with high amplitudes were generated in the sub-laminate $[0_4]_T$ in the $\theta = 90°$ direction and were utilized to identify the film-inserted area in this study. Conversely, the flexural stiffness of the sub-laminate $[0_4]_T$ in the $\theta = 0°$ direction was not so small that the standing waves exhibit high amplitudes enough to characterize the delamination. This resulted in misidentifying the delamination for $\theta = 0°$. Based on the above discussion, incorporating other ultrasonic features enough sensitive to the delamination into the objective function is required to quantitatively evaluate the delamination regardless of the incidence angles.

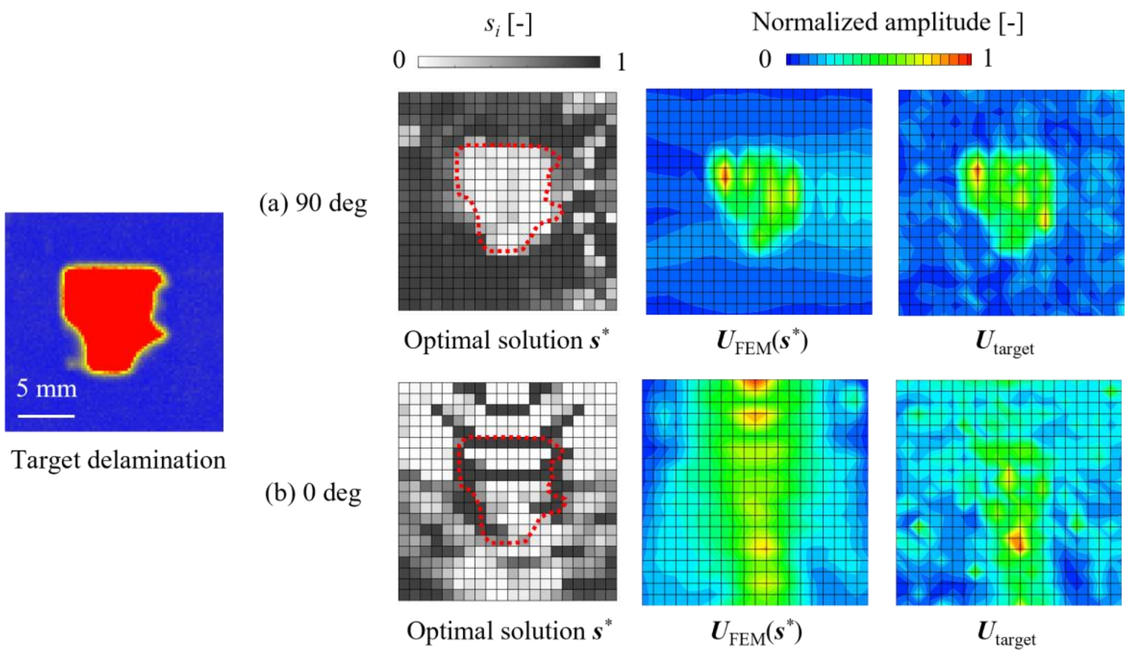

Figure 7: Optimal solutions of the damage parameter $\boldsymbol{s}^*$ and maximum amplitude distribution $\boldsymbol{U}_{\mathrm{FEM}}(\boldsymbol{s}^*)$ compared to the target delamination and target data $\boldsymbol{U}_{\mathrm{target}}$.

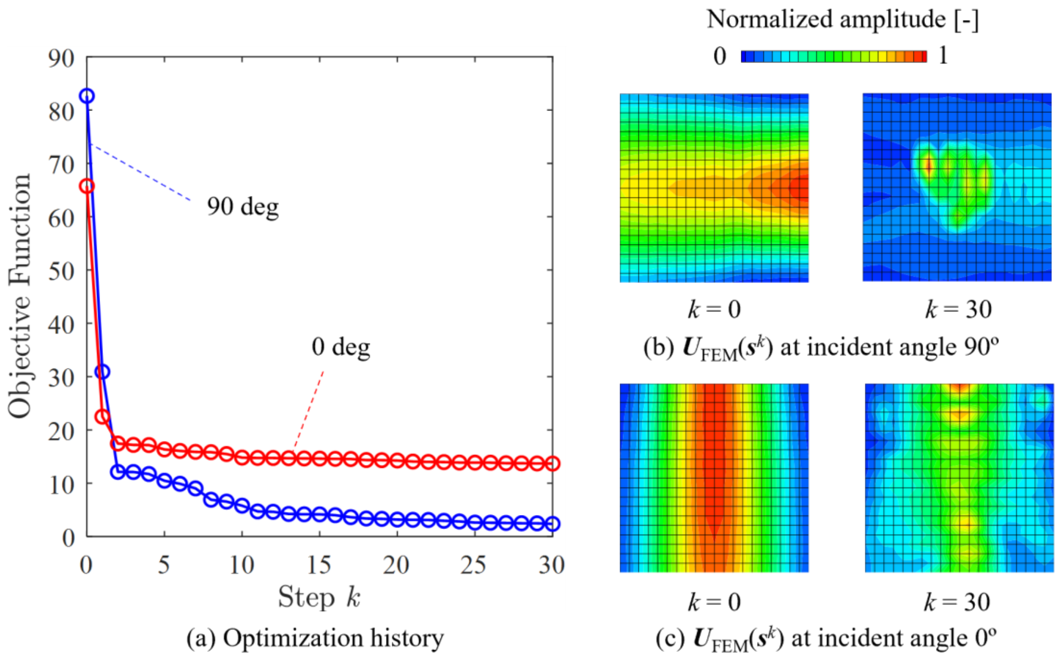

Figure 8: Optimization history of (a) the objective function, and the maximum amplitude maps $\boldsymbol{U}_{\mathrm{FEM}}(\boldsymbol{s}^k)$ for optimization steps k = 0 and 30 at the incident angles (b) 90° and (c) 0°.

4.2 Discussion of the objective function

The dispersion nature of Lamb waves (e.g., velocity, wavenumber, etc.) is considered appropriate as the ultrasonic features to be evaluated in the objective function because the A0 mode phase was delayed in the delaminated region as shown in Figure 2. Therefore, in this section, the delamination was estimated by evaluating all signals of the visualized Lamb wave propagation that included all effects related to the dispersion nature. For simplicity, the numerical experiment was performed in this section. The target delamination was the central 10 mm × 10 mm (10 × 10 elements) region in the design domain, and the target ultrasonic features $\boldsymbol{U}_{\mathrm{target}}$ were set to the numerical results obtained by the dynamic finite element analysis.

The objective function was set to the sum of the squared error between all the out-of-plane displacements calculated in the estimated and target damage parameter distributions. Figure 9 shows the optimal solution $\boldsymbol{s}^*$ compared to the target. In the case of θ = 0°, the damage parameters in the delaminated region were smaller than that in the intact region, and the delaminated region was successfully identified. This result suggests that the present method can estimate delamination even at θ = 0° if the ultrasonic features other than maximum amplitudes are extracted and incorporated into the objective function. Conversely, unlike the identification results in Section 4.1, the target delamination was not identified at θ = 90°, which resulted from the complex optimization problem due to too much data to be evaluated. Therefore, improving the sensitivity of the objective function by investigating ultrasonic features sensitive to delamination and combining some of them appropriately is important to apply the present method to identifying delamination regardless of incidence angles.

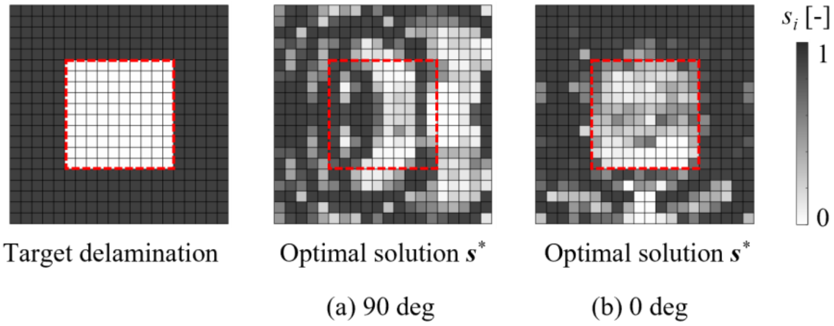

Figure 9: Optimal solutions of the damage parameter $\boldsymbol{s}^*$ using all waveforms of out-of-plane displacement at each node in design domain as the objective function.

5 CONCLUDING REMARKS

In this study, the topology-optimization-based damage identification method combined with the ultrasonic visualization was applied to quantitatively evaluating the film-inserted region in the cross-ply laminate to investigate the feasibility of the method. In the present method, the damage parameters were set to the internal residual strength valuables governing the traction of the cohesive elements. The damage parameter distribution was optimized by mathematical programming so that the experimentally visualized Lamb wave propagation was reproduced in the inverse analysis model. When the maximum amplitudes were adopted as the ultrasonic feature to be evaluated in the objective function, the complex shape of the film-inserted area was successfully identified by utilizing the standing waves with high amplitudes in the delaminated region at $\theta = 90°$. This result demonstrates that the present method can evaluate delamination quantitatively based on Lamb wave propagation mechanisms. Conversely, the film-inserted area was not identified at $\theta = 0°$ because the maximum amplitudes were not sensitive to delamination.

The target delamination was successfully estimated at $\theta = 0°$ by evaluating all waveforms included in the visualized Lamb wave propagation as the objective function. This result shows that delamination can be identified regardless of the incidence angles by incorporating ultrasonic features related to the Lamb wave dispersive nature, such as velocity and wavenumber, into the objective function. In future work, clarifying ultrasonic features sensitive to delamination and setting the objective function appropriately based on the findings are required.

ACKNOWLEDGEMENTS

This work was supported by JSPS KAKENHI Grant Number JP20J21916. The authors would like to thank Dr. Shin-ichi Takeda and Dr. Tetsuo Yasuoka (Japan Aerospace Exploration Agency) for their technical support during the study.

REFERENCES

[1] S. Yashiro, J. Takatsubo and N. Toyama, An NDT technique for composite structures using visualized Lamb-wave propagation, *Composite Science and Technology*, **67**, 15–16, 2007, pp. 3202–3208 (doi: 10.1016/j.compscitech.2007.04.006).

[2] H. Sohn, D. Dutta, J.Y. Yang, H.J. Park, M. DeSimio, S. Olson and E. Swenson, Delamination detection in composites through guided wave field image processing, *Composite Science and Technology*, **71**, 9, 2011, pp. 1250–1256 (doi: 10.1016/j.compscitech.2011.04.011).

[3] J.L. Rose, *Ultrasonic waves in solid media*, Cambridge University Press, Cambridge (UK), 1999.

[4] C.C. Chia, S.Y. Lee, M.Y. Harmin, Y. Choi and J.R. Lee, Guided ultrasonic waves propagation imaging: a review, *Measurement Science and Technology*, **34**, 2023, 052001 (doi: 10.1088/1361-6501/acae27).

[5] M. P. Bendsøe and N. Kikuchi, Generating optimal topologies in structural design using a homogenization method, *Computer Methods in Applied Mechanics and Engineering*, **71**, 2, 1988, pp. 197–224 (doi: 10.1016/0045-7825(88)90086-2).

[6] H. Niemann, J. Morlier, A. Shahdin and Y. Gourinat. Damage localization using experimental modal parameters and topology optimization, *Mechanical Systems and Signal Processing*, **24**, 3, 2010, pp. 636–652 (doi: 10.1016/j.ymssp.2009.10.022).

[7] K. Ryuzono, S. Yashiro, H. Nagai and N. Toyama, Topology optimization-based damage identification using visualized ultrasonic wave propagation, *Materials*, **13**, 1, 2020, 33 (doi: 10.3390/ma13010033).

[8] K. Ryuzono, S. Yashiro, S. Onodera and N. Toyama. Performance evaluation of crack identification using density-based topology optimization for experimentally visualized ultrasonic wave propagation, *Mechanics of Materials*, **172**, 2022, 104406 (doi: 10.1016/j.mechmat.2022.104406).

[9] T. Hayashi and K. Kawashima, Multiple reflections of Lamb waves at a delamination, *Ultrasonics*, **40**, 1–8, 2002, pp. 193–197 (doi: 10.1016/S0041-624X(02)00136-1).

[10] P. Kudela, T. Wandowski, P. Malinowski and W. Ostachowicz, Application of scanning laser Doppler vibrometry for delamination detection in composite structures, *Optics and Lasers in Engineering*, **99**, 2017, pp. 46–57 (doi: 10.1016/j.optlaseng.2016.10.022).

[11] K. Ryuzono, S. Yashiro, S. Onodera and N. Toyama, Lamb wave mode conversion and multiple-reflection mechanisms for simply and reliably evaluating delamination in composite laminates, *Advanced Composite Materials*, in press (doi: 10.1080/09243046.2022.2146564).

[12] P.H. Geubelle and J.S. Baylor, Impact-induced delamination of composites: a 2D simulation, *Composites Part B: Engineering*, **29**, 5, 1998, pp. 589–602 (doi: 10.1016/S1359-8368(98)00013-4).

[13] S. Yashiro, T. Agata and A. Yoshimura. A new approach for evaluating crack growth resistance curve of mode II delamination by doubly end-notched tension tests, *Advanced Composite Materials*, **27**, 2, 2018, pp. 119–133 (doi: 10.1080/09243046.2017.1373384).

[14] S. Yashiro, K. Ogi, A. Yoshimura and Y. Sakaida, Characterization of high-velocity impact damage in CFRP laminates: Part II – prediction by smoothed particle hydrodynamics, *Composites Part A: Applied Science and Manufacturing*, **56**, 2014, pp. 308–318 (doi: 10.1016/j.compositesa.2013.04.012).